# Pair production of Higgs boson in NMSSM at the LHC with the next-to-lightest $CP$-even Higgs boson being SM-like*

Zhaoxia Heng(衡朝霞)[1)] Xue Gong(巩雪) Haijing Zhou(周海静)[2)]
College of Physics and Materials Science, Henan Normal University, Xinxiang 453007, China

**Abstract:** The next-to-minimal supersymmetric standard model (NMSSM) more naturally accommodates a Higgs boson with a mass of approximately 125 GeV than the minimal supersymmetric standard model (MSSM). In this work, we assume that the next-to-lightest $CP$-even Higgs boson $h_2$ is the SM-like Higgs boson $h$, whereas the lightest $CP$-even Higgs boson $h_1$ is dominantly singlet-like. We discuss the $h_1h_1$, $h_2h_2$, and $h_1h_2$ pair production processes via gluon-gluon fusion at the LHC for an collision energy of 14 TeV, and we consider the cases in which one Higgs boson decays to $b\bar{b}$ and the other decays to $\gamma\gamma$ or $\tau^+\tau^-$. We find that, for $m_{h_1} \lesssim 62$ GeV, the cross section of the $gg \to h_1h_1$ process is relatively large and maximally reaches 5400 fb, and the production rate of the $h_1h_1 \to b\bar{b}\tau^+\tau^-$ final state can reach 1500 fb, which make the detection of this final state possible for future searches of an integrated luminosity of 300 and 3000 fb$^{-1}$. This is mainly due to the contributions from the resonant production process $pp \to h_2 \to h_1h_1$ and the relatively large branching ratio of $h_1 \to b\bar{b}$ and $h_1 \to \tau^+\tau^-$. The cross sections of the $pp \to h_2h_2$ and $pp \to h_1h_2$ production processes maximally reach 28 fb and 133 fb, respectively.

**Keywords:** next-to-Minimal supersymmetric standard model (NMSSM), SM-like Higgs boson, Higgs pair production

**PACS:** 14.80.Da, 12.60.Jv, 14.80.Ly **DOI:** 10.1088/1674-1137/42/7/073103

## 1 Introduction

In July 2012, the ATLAS and CMS collaborations at the Large Hadron Collider (LHC) at CERN reported the observation of a new boson with a mass of approximately 125 GeV [1]. After this discovery, which marked a milestone in particle physics, the extensive amount of data accumulated by both experiments [2] have established that the properties of the new boson are consistent with those predicted by the standard model (SM). Since the discovery of the Higgs boson, much work has been done to study its properties by measuring all the possible production channel cross sections and decay rates. In particular, it has been demonstrated that, among all the possible production modes, double Higgs production is a sensitive probe for new physics [3–8].

At leading order in the SM, Higgs pair production at the LHC happens through the gluon–gluon fusion $gg \to hh$ process [9, 10]. The SM cross section of such a process receives contributions from loops mediated by heavy quarks, which induce box and triangle diagrams ($gg \to h^* \to hh$). The amplitudes of these two types of diagrams interfere with each other destructively, thus leading to a rather small cross section. In new physics models, such as low energy supersymmetric models, both box and triangle diagrams receive additional contributions from the loops mediated by the third generation of squarks. Moreover, the triangle diagrams are correlated with the trilinear Higgs coupling, which plays an important role in the reconstruction of the Higgs potential [11]. Therefore, the $gg \to hh$ process is particularly sensitive to new physics contributions.

Among new physics models, the next-to-minimal supersymmetric standard model (NMSSM) has attracted considerable attention [12], as it more naturally accommodates a Higgs boson with a mass near 125 GeV than the minimal supersymmetric standard model (MSSM). Compared with the MSSM, the NMSSM introduces an additional singlet Higgs field $\hat{S}$. Because of the coupling between singlet and doublet Higgs fields in the superpotential, the mass of the SM-like Higgs boson can be enhanced at tree-level. Furthermore, the mixing between singlet and doublet Higgs fields can also increase the mass of the Higgs boson when the next-to-lightest $CP$-even Higgs boson corresponds to the SM-like Higgs boson [13–15]. These two contributions can easily increase the

Received 6 April 2018, Published online 28 May 2018
∗ Supported by National Natural Science Foundation of China (11705048)
1) E-mail: zxheng@htu.edu.cn
2) E-mail: zhouhaijing@htu.edu.cn
©2018 Chinese Physical Society and the Institute of High Energy Physics of the Chinese Academy of Sciences and the Institute of Modern Physics of the Chinese Academy of Sciences and IOP Publishing Ltd

mass of the Higgs boson to 125 GeV without any large radiative corrections. In this work, we only consider the scenario in which the next-to-lightest $CP$-even Higgs boson acts as the SM-like Higgs boson $h$.

Due to the presence of the additional superfield $\hat{S}$, the NMSSM contains three $CP$-even Higgs particles $h_i$ ($i$= 1,2,3), which respect the convention $m_{h_1}<m_{h_2}<m_{h_3}$. In this work, we assume that $h_2$ acts as the SM-like Higgs boson $h$, and $h_1$ is dominantly singlet-like considering the constraints for Higgs searches from LEP, Tevatron and LHC. We study the main di-Higgs production process at the LHC, the gluon–gluon fusion production of $h_1h_1$, $h_2h_2$, and $h_1h_2$ Higgs pairs. At present, the possible most promising detection channels for Higgs pair production at the LHC are $hh\to b\bar{b}\gamma\gamma$, $hh\to b\bar{b}\tau^+\tau^-$ and $hh\to b\bar{b}W^+W^-$ [16]. However, due to the weak interaction between the lightest $CP$-even Higgs $h_1$ and $W^+W^-$, we will focus on the $b\bar{b}\gamma\gamma$ and $b\bar{b}\tau^+\tau^-$ channels.

This work is organized as follows. In Section 2 we briefly introduce the Higgs sector of the NMSSM. In Section 3 we scan over the NMSSM parameter space by considering various experimental constraints; then we calculate the cross sections of $h_1h_1$, $h_2h_2$, and $h_1h_2$ di-Higgs gluon-fusion production processes and we also discuss the production rates for the $b\bar{b}\gamma\gamma$ and $b\bar{b}\tau^+\tau^-$ final states. Finally, we present our conclusions in Section 4.

## 2 Higgs sector in NMSSM

As in the MSSM, the NMSSM contains two doublet Higgs superfields $\hat{H}_u$ and $\hat{H}_d$; however, in addition to the MSSM, the NMSSM introduces one gauge singlet superfield $\hat{S}$. As a consequence, the Higgs sector has a richer structure in the NMSSM than in the MSSM. To avoid the occurrence of dimensionful parameters in the superpotential, a discrete $Z_3$-symmetry is imposed. The corresponding superpotential and soft-breaking terms in the Higgs sector of the $Z_3$-invariant NMSSM are given by Eqs. (1) and (2) [12, 17]:

$$\begin{aligned} W_{\rm NMSSM} &= Y_u\hat{Q}\cdot\hat{H}_u\hat{U}-Y_d\hat{Q}\cdot\hat{H}_d\hat{D}-Y_e\hat{L}\cdot\hat{H}_d\hat{E} \\ &\quad +\lambda\hat{H}_u\cdot\hat{H}_d\hat{S}+\frac{1}{3}\kappa\hat{S}^3, \end{aligned} \tag{1}$$

$$\begin{aligned} V_{\rm soft}^{\rm NMSSM} &= \tilde{m}_u^2|H_u|^2+\tilde{m}_d^2|H_d|^2+\tilde{m}_S^2|S|^2 \\ &\quad +\left(A_\lambda\lambda SH_u\cdot H_d+\frac{A_\kappa}{3}\kappa S^3+{\rm h.c.}\right). \end{aligned} \tag{2}$$

where $\hat{Q}$, $\hat{U}$, $\hat{D}$, $\hat{L}$, and $\hat{E}$ are chiral superfields with $Y_u$,$Y_d$,$Y_e$ being their Yukawa coupling coefficients; $\lambda$ and $\kappa$ denote dimensionless coupling coefficients; and $\tilde{m}_u$, $\tilde{m}_d$, $\tilde{m}_S$, $A_\lambda$, and $A_\kappa$ are the soft-breaking parameters. When the electroweak symmetry is broken, the parameters $\tilde{m}_u$, $\tilde{m}_d$, and $\tilde{m}_S$ are expressed in terms of $m_Z$, $\tan\beta\equiv v_u/v_d$, and $\mu\equiv\lambda v_s$ with $v_u$, $v_d$, and $v_s$ being the vacuum expectation values (VEV) of the Higgs fields $H_u$, $H_d$, and $S$. Thus, at tree level, the Higgs sector of the NMSSM can be represented by six independent parameters given by Eq. (3):

$$\lambda, \quad \kappa, \quad \tan\beta, \quad \mu, \quad M_A, \quad A_\kappa, \tag{3}$$

with $M_A^2=\frac{2\mu(A_\lambda+\kappa v_s)}{\sin 2\beta}$.

In the NMSSM, $H_u$, $H_d$, and $S$ are given by Eq. (4):

$$\begin{aligned} H_u&=\begin{pmatrix} H_u^+ \\ v_u+\dfrac{\phi_u+i\varphi_u}{\sqrt{2}} \end{pmatrix}, \quad H_d=\begin{pmatrix} v_d+\dfrac{\phi_d+i\varphi_d}{\sqrt{2}} \\ H_d^- \end{pmatrix}, \\ S&=v_s+\frac{1}{\sqrt{2}}(\sigma+i\xi). \end{aligned} \tag{4}$$

By diagonalizing the corresponding mass matrices, we get the Higgs mass eigenstates as in Eq. (5):

$$\begin{aligned} &\begin{pmatrix} h_1 \\ h_2 \\ h_3 \end{pmatrix} = U^H\begin{pmatrix} \phi_u \\ \phi_d \\ \sigma \end{pmatrix}, \quad \begin{pmatrix} a_1 \\ a_2 \\ G^0 \end{pmatrix}=U^A\begin{pmatrix} \varphi_u \\ \varphi_d \\ \xi \end{pmatrix}, \\ &\begin{pmatrix} H^+ \\ G^+ \end{pmatrix} = U^C\begin{pmatrix} H_u^+ \\ H_d^+ \end{pmatrix}. \end{aligned} \tag{5}$$

Here, $h_i$ (with $i$ = 1,2,3) denotes the physical $CP$-even neutral scalars with $m_{h_1}<m_{h_2}<m_{h_3}$; $a_i$ (with $i$=1,2) denotes the physical $CP$-odd neutral scalars with $m_{a_1}<m_{a_2}$; $H^+$ is the physical charged Higgs boson; and $G^0$ and $G^+$ are the Goldstone bosons absorbed by the $Z$ and $W$ bosons, respectively.

Because of the coupling $\lambda\hat{H}_u\cdot\hat{H}_d\hat{S}$ in the superpotential, the mass of the SM-like Higgs boson $h$ at tree level has the following dependencies:

$$m_{h,tree}^2=m_Z^2\cos^2 2\beta+\lambda^2v^2\sin^2 2\beta. \tag{6}$$

As shown by Eq. (6), the SM-like Higgs boson ($h$) mass increases as $\lambda$ increases and $\tan\beta$ decreases. Moreover, the mixing between singlet and doublet Higgs fields can also significantly alter the $h$ mass. In particular, the mixing will pull down the mass when $h_1$ acts as $h$, whereas it will push up the mass when $h_2$ acts as $h$ [13, 14]. Therefore, when $h_2$ plays the role of the SM-like Higgs boson, both the additional tree-level contributions and the effect of Higgs doublet-singlet mixing can increase the $h$ mass; such a phenomenon makes the large radiative corrections from top-squark loops unnecessary to predict a Higgs boson with a mass near 125 GeV.

## 3 Calculations and numerical results

### 3.1 Scanning strategy of the parameter space

We perform a comprehensive scan over the parameter space of the NMSSM by using the package NMSSMTools [18]. We constrain the mass of the gluino and the soft breaking parameters in the first two generations of

the squark sector to be equal to 2 TeV. Moreover, we assume a common value denoted by $m_{\tilde{l}}$ for all soft breaking parameters in the slepton sector. The parameter space considered in the scan is represented by Eq. (7):

$$\begin{aligned}
&0<\lambda,\kappa\leqslant 0.75, \quad 2\leqslant\tan\beta\leqslant 60,\\
&100\ \text{GeV}\leqslant\mu\leqslant 1\ \text{TeV}, \quad 50\ \text{GeV}\leqslant M_A\leqslant 2\ \text{TeV},\\
&|A_\kappa|\leqslant 2\text{TeV}, \quad 100\ \text{GeV}\leqslant m_{\tilde{l}}\leqslant 1\ \text{TeV},\\
&100\ \text{GeV}\leqslant M_{Q_3}\leqslant 2\ \text{TeV},\\
&100\ \text{GeV}\leqslant M_{U_3}(=M_{D_3})\leqslant 2\ \text{TeV},\\
&|A_t(=A_b)|\leqslant\min(3\sqrt{M_{Q_3}^2+M_{U_3}^2},5\ \text{TeV}),\\
&20\text{GeV}\leqslant M_1\leqslant 500\ \text{GeV}, 100\ \text{GeV}\leqslant M_2\leqslant 1\ \text{TeV}. \quad (7)
\end{aligned}$$

In addition to the constraints implemented in the package NMSSMTools we also consider the following:

1) Constraints from the direct searches for the Higgs boson at LEP, Tevatron, and LHC. We adopt the package HiggsSignals for the fit of the 125 GeV Higgs data [19] and the package HiggsBounds for the searches for non-standard Higgs bosons at colliders [20].

2) Constraints from direct searches for sparticles at LHC Run-I and Run-II. We use the packages FastLim [21] and SModelS [22] to implement such constraints. In particular, the results of the experimental searches for gluino and squarks are implemented in the package FastLim, whereas those of sleptons and electroweakinos searches are implemented in the SModelS package. Efficiencies or upper bounds on the sparticle productions can be obtained to limit the parameter space of the NMSSM.

3) Constraints from the searches for electroweakinos and top-squarks at the LHC Run-II. The surviving samples that satisfy the constraints from FastLim and SModelS are further tested by detailed Monte Carlo simulations. In detail, we use MadGraph/MadEvent [23] to simulate events at the parton level and Pythia [24] to do parton showers and hadronization, then we put the events into Delphes [25] to do detector simulation. Finally, we implement the ATLAS and CMS searches within CheckMATE [26] to decide whether each parameter point in our scenario is allowed or not.

### 3.2 Numerical results

In our numerical calculation we take $m_t = 173.2$ GeV, $m_b = 4.18$ GeV, $m_Z = 91.19$ GeV [27], and take the renormalization and factorization scales to be the invariant mass of the Higgs pair. We select the samples for 122 GeV $\leqslant m_h \leqslant$ 128 GeV and require the next-to-lightest $CP$-even Higgs boson ($h_2$) to be the SM-like Higgs boson $h$.

According to the NMSSM scenario, the Higgs pair production processes possibly available at the LHC happen via gluon–gluon fusion, as shown in Fig. 1. Different from the SM, in the NMSSM the gluon–gluon fusion receives additional contributions from the loops mediated by the third generation of squarks. We checked that we can reproduce the results in the SM and MSSM presented in Refs. [9] and [28]. In the numerical calculations, for an LHC collision energy of 14 TeV, we find that the cross section of the $gg\to hh$ process in the SM scenario is 18.7 fb at $m_h = 125$ GeV.

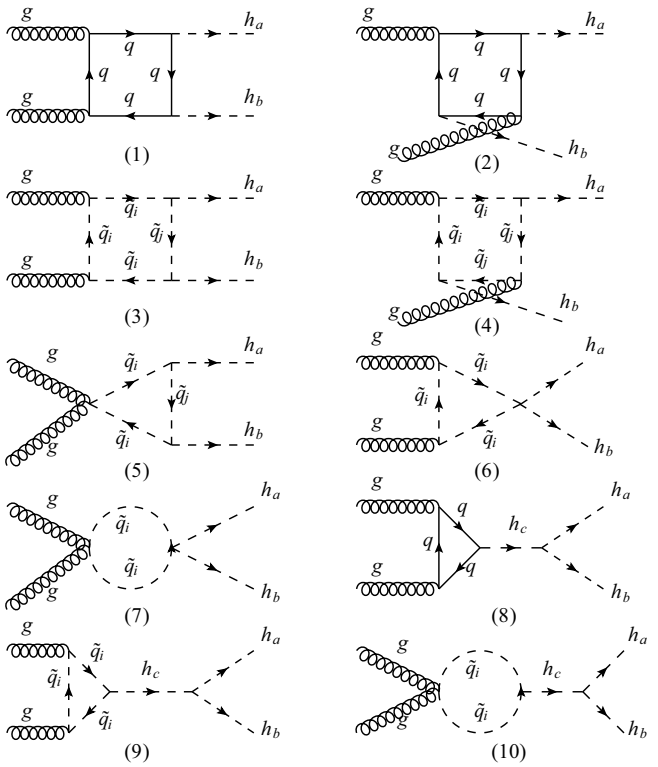


Fig. 1. Feynman diagrams of Higgs pair production in the NMSSM with $a$,$b$=1,2 and $c$=1,2,3.

Figure 2 shows the cross sections of the $h_1h_1$ (left), $h_2h_2$ (middle), and $h_1h_2$ (right) pair production processes. The cross section of the process $pp\to h_1h_1$ (left-hand panel) assumes values mainly divided into two regions: for $m_{h_1}\lesssim 62$ GeV, the cross section is relatively large and it can maximally reach 5400 fb. This is because the rare decay $h_2\to h_1h_1$ is open when $m_{h_1}\lesssim 62$ GeV. As can be clearly seen from Fig. 3, which shows the cross section of the $pp\to h_1h_1$ process as a function of the branching ratio of the decay $h_2\to h_1h_1$, the $pp\to h_1h_1$ cross section increases as the $h_2\to h_1h_1$ branching ratio increases.

The plot in the middle panel of Fig. 2 indicates that the cross section of the $pp\to h_2h_2$ process can maximally reach 28 fb, which is 1.5 times larger than the SM prediction. The enhancement mainly originates from the contributions of diagrams (3), (4), and (5) in Fig. 1. For lighter $m_{\tilde{t}_1}$ and larger values of $A_t$ the cross section is

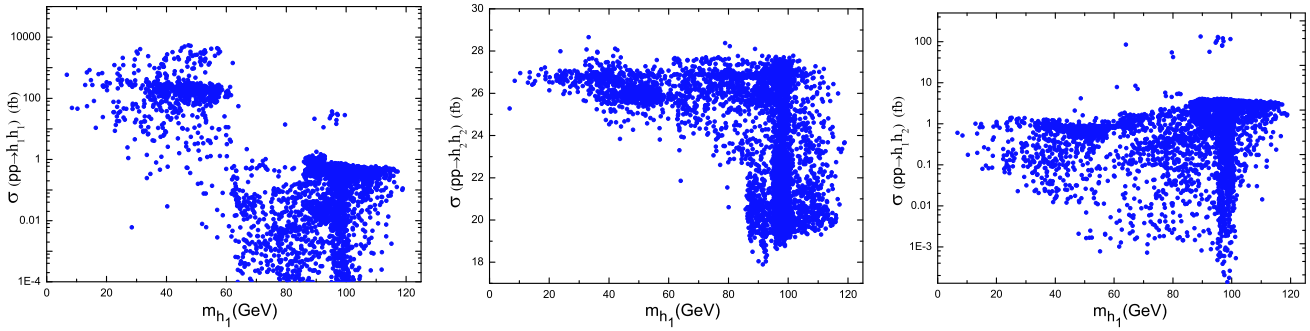


Fig. 2. (color online) Cross sections of Higgs pair production processes in the final states $h_1h_1$, $h_2h_2$, and $h_1h_2$.

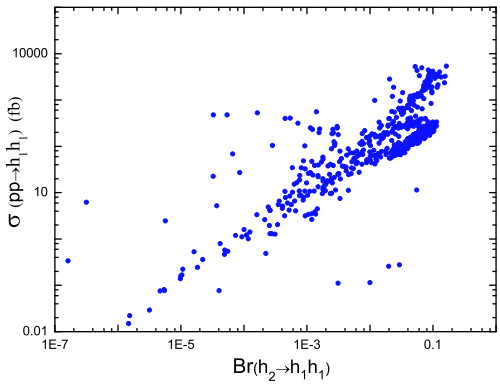


Fig. 3. (color online) Cross section of the Higgs pair production process in the final state $h_1h_1$ as a function of the $h_2\to h_1h_1$ branching ratio.

larger, which is in agreement with the results reported in Ref. [7].

From the right-hand panel of Fig. 2 it is seen that, for the majority of the surviving samples, the cross section of $pp\to h_1h_2$ is less than 10 fb; this mainly because $h_1$ is dominantly singlet-like. However, for a few surviving samples, the cross section can exceed 100 fb and reach 133 fb at maximum. In these cases, the heaviest $CP$-even Higgs $h_3$ is relatively light with a mass of approximately 500 GeV, and $h_3$ is produced on-shell with the branching ratio to $h_1h_2$ being about 10%. It is important to notice that the mass of the heavy Higgs boson near 500 GeV for $\tan\beta\lesssim 5$ in the MSSM is not excluded by experimental results based on the LHC Run-II data [29, 30].

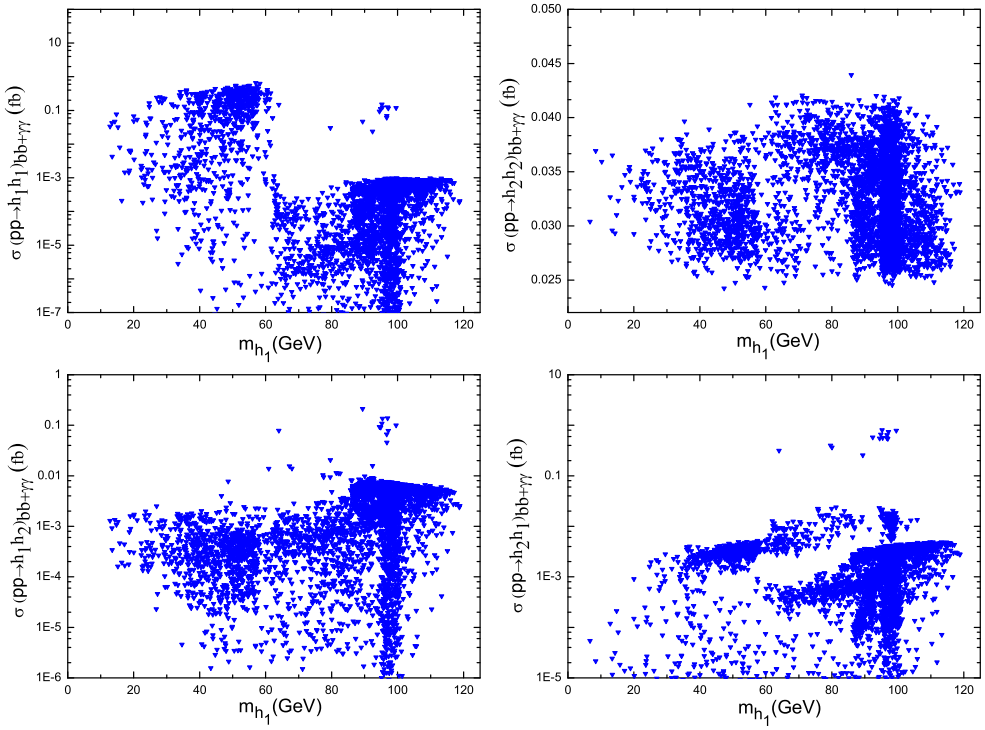


Fig. 4. (color online) Production rates of Higgs pair production processes in the final states $h_1h_1\to b\bar{b}\gamma\gamma$, $h_2h_2\to b\bar{b}\gamma\gamma$, $h_1h_2\to b\bar{b}\gamma\gamma$, and $h_2h_1\to b\bar{b}\gamma\gamma$.

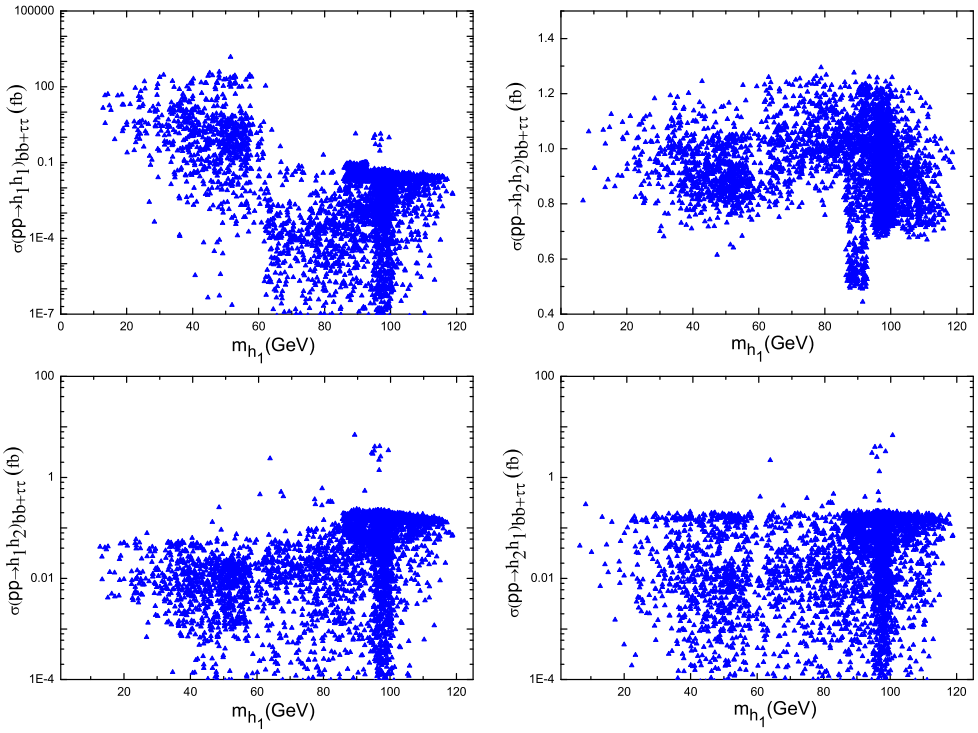


Fig. 5. (color online) Production rates of Higgs pair production processes in the final states $h_1h_1 \to b\bar{b}\tau^+\tau^-$, $h_2h_2 \to b\bar{b}\tau^+\tau^-$, $h_1h_2 \to b\bar{b}\tau^+\tau^-$, and $h_2h_1 \to b\bar{b}\tau^+\tau^-$.

Since the discovery potential of the Higgs boson depends on the decay spectrum of the Higgs boson, we now consider the $h_1h_1$, $h_2h_2$, and $h_1h_2$ di-Higgs production processes with one Higgs boson decaying to $b\bar{b}$ and the other one decaying to either $\gamma\gamma$ or $\tau^+\tau^-$. In Fig. 4 and Fig. 5 we show the production rates of the final states $b\bar{b}\gamma\gamma$ and $b\bar{b}\tau^+\tau^-$, respectively. As can be seen, the production rate of the process $h_1h_1 \to b\bar{b}\tau^+\tau^-$ is relatively large for $m_{h_1} \lesssim 62$ GeV, and it can maximally reach 1500 fb. This is because, for most of the surviving samples, the $h_1 \to b\bar{b}$ and $h_1 \to \tau^+\tau^-$ branching ratios are close to 90% and 8%, respectively.

Both the ATLAS and CMS collaborations performed searches for 125 GeV Higgs pair production in the final states $b\bar{b}b\bar{b}$, $b\bar{b}\tau^+\tau^-$ and $b\bar{b}\gamma\gamma$. Based on the data collected at $\sqrt{s} = 13$ TeV with an integrated luminosity of 35.9 fb$^{-1}$, the observed 95% CL upper limit for the $b\bar{b}b\bar{b}$ final state is 147 fb, corresponding to 13 times the SM prediction [31], for the $b\bar{b}\tau^+\tau^-$ final state it is 75.4 fb, corresponding to 30 times the SM prediction [32], and for the $b\bar{b}\gamma\gamma$ final state it is 1.67 fb, corresponding to 19.2 times the SM prediction [33]. For the present integrated luminosity of the LHC, the Higgs pair production in the considered scenario of NMSSM cannot be directly detected. Due to the large production rate of the process $pp \to h_1h_1 \to b\bar{b}\tau^+\tau^-$, for future searches with an integrated luminosity of 300 and 3000 fb$^{-1}$, Higgs pair production for the $h_1h_1 \to b\bar{b}\tau^+\tau^-$ final state may be detected.

## 4 Conclusion

Because of the mixing effect of Higgs doublet-singlet fields, and the coupling effect between Higgs doublet and singlet fields in the superpotential, the NMSSM more naturally accommodates a Higgs boson with a mass of approximately 125 GeV. We assume that the next-to-lightest $CP$-even Higgs boson $h_2$ plays the role of the SM-like Higgs boson. In this scenario the lightest $CP$-even Higgs boson $h_1$ is dominantly singlet-like and it can be much lighter than 125 GeV. In this work, we discussed the $h_1h_1$, $h_2h_2$, and $h_1h_2$ pair production processes via gluon-gluon fusion at the LHC for an collision energy of 14 TeV. In addition, we studied the production rate of such di-Higgs events in which one Higgs boson decays to $b\bar{b}$ and the other to either $\gamma\gamma$ or $\tau^+\tau^-$. We found that, for $m_{h_1} \lesssim 62$ GeV, the cross section of the $gg \to h_1h_1$ production process is relatively large and maximally reaches 5400 fb, and that the production rate of the $h_1h_1 \to b\bar{b}\tau^+\tau^-$ final state can reach 1500 fb. These results are mainly due to the contributions from the resonant production process $pp \to h_2 \to h_1h_1$and the relatively

large branching ratio of the $h_1 \to b\bar{b}$ and $h_1 \to \tau^+\tau^-$ decays. The cross sections of the $pp \to h_2h_2$ and $pp \to h_1h_2$ production processes maximally reach 28 fb and 133 fb, respectively. Therefore, for future searches with an integrated luminosity of 300 and 3000 fb$^{-1}$, Higgs pair production for the $h_1h_1 \to b\bar{b}\tau^+\tau^-$ final state may be detected.

## References


1 G. Aad et al (ATLAS Collaboration), Phys. Lett. B, **716**: 1 (2012); S. Chatrchyan et al (CMS Collaboration), Phys. Lett. B, **716**: 30 (2012)

2 G. Aad et al (ATLAS Collaboration), Eur. Phys. J. C, **76**(1):, 6 (2016) [arXiv:1507.04548 [hep-ex]]; V. Khachatryan et al (CMS Collaboration), Eur. Phys. J. C, **75**(5): 212 (2015) [arXiv:1412.8662 [hep-ex]]; S. Chatrchyan et al (CMS Collaboration), Phys. Rev. Lett., **110**(8): 081803 (2013) [arXiv:1212.6639 [hep-ex]]; G. Aad et al (ATLAS Collaboration), Phys. Lett. B, **726**: 120 (2013) [arXiv:1307.1432 [hep-ex]]

3 M. J. Dolan, C. Englert, and M. Spannowsky, Phys. Rev. D, **87**(5): 055002 (2013) [arXiv:1210.8166 [hep-ph]]; S. Dawson, A. Ismail, and I. Low, Phys. Rev. D, **91**(11): 115008 (2015) [arXiv:1504.05596 [hep-ph]]; H. J. He, J. Ren, and W. Yao, Phys. Rev. D, **93**(1): 015003 (2016) [arXiv:1506.03302 [hep-ph]]; G. D. Kribs and A. Martin, Phys. Rev. D, **86**: 095023 (2012) [arXiv:1207.4496 [hep-ph]]

4 M. Carena, Z. Liu, and M. Riembau, arXiv:1801.00794 [hep-ph]; J. H. Kim, Y. Sakaki, and M. Son, arXiv:1801.06093 [hep-ph]; L. Bian, N. Chen, and Y. Jiang, Int. J. Mod. Phys. A, **32**(34): 1746002 (2017) [arXiv:1712.01632 [hep-ph]]; J. Ren, R. Q. Xiao, M. Zhou, Y. Fang, H. J. He, and W. Yao, arXiv:1706.05980 [hep-ph]; I. M. Lewis and M. Sullivan, Phys. Rev. D, **96**(3): 035037 (2017) [arXiv:1701.08774 [hep-ph]]; S. Dawson and M. Sullivan, arXiv:1711.06683 [hep-ph]; K. Nakamura, K. Nishiwaki, K. y. Oda, S. C. Park, and Y. Yamamoto, Eur. Phys. J. C, **77**(5): 273 (2017) [arXiv:1701.06137 [hep-ph]]

5 C. Han, X. Ji, L. Wu, P. Wu, and J. M. Yang, JHEP, **1404**: 003 (2014) [arXiv:1307.3790 [hep-ph]]; X. F. Han, L. Wang, and J. M. Yang, Nucl. Phys. B, **825**: 222 (2010) [arXiv:0908.1827 [hep-ph]]; X. F. Han, L. Wang, and J. M. Yang, Mod. Phys. Lett. A, **31**(31): 1650178 (2016) [arXiv:1509.02453 [hep-ph]]; J. Cao, D. Li, L. Shang, P. Wu, and Y. Zhang, JHEP, **1412**: 026 (2014) [arXiv:1409.8431 [hep-ph]]; Z. Heng, L. Shang, Y. Zhang, and J. Zhu, JHEP, **1402**: 083 (2014) [arXiv:1312.4260 [hep-ph]]

6 U. Ellwanger, JHEP, **1308**: 077 (2013) [arXiv:1306.5541 [hep-ph]]

7 J. Cao, Z. Heng, L. Shang, P. Wan, and J. M. Yang, JHEP, **1304**: 134 (2013) [arXiv:1301.6437 [hep-ph]]

8 P. Huang, A. Joglekar, M. Li, and C. E. M. Wagner, arXiv:1711.05743 [hep-ph]

9 A. Djouadi, W. Kilian, M. Muhlleitner, and P. M. Zerwas, Eur. Phys. J. C, **10**: 45 (1999) [hep-ph/9904287]

10 T. Plehn, M. Spira, and P. M. Zerwas, Nucl. Phys. B, **479**: 46 (1996) Erratum: [Nucl. Phys. B, **531**: 655 (1998)] [hep-ph/9603205]; E. W. N. Glover and J. J. van der Bij, Nucl. Phys. B, **309**: 282 (1988)

11 J. Baglio et al, JHEP, **1304**: 151 (2013) [arXiv:1212.5581 [hep-ph]]; D. Y. Shao, C. S. Li, H. T. Li, and J. Wang, JHEP, **1307**: 169 (2013) [arXiv:1301.1245 [hep-ph]]

12 U. Ellwanger, C. Hugonie, and A. M. Teixeira, Phys. Rept., **496**: 1 (2010) [arXiv:0910.1785]

13 J. J. Cao, Z. X. Heng, J. M. Yang, Y. M. Zhang, and J. Y. Zhu, JHEP, **1203**: 086 (2012) [arXiv:1202.5821 [hep-ph]]

14 Z. Kang, J. Li, and T. Li, JHEP, **1211**: 024 (2012) [arXiv:1201.5305 [hep-ph]]

15 J. Cao, Y. He, L. Shang, W. Su, and Y. Zhang, JHEP, **1608**: 037 (2016) [arXiv:1606.04416 [hep-ph]]; J. Cao, Y. He, L. Shang, W. Su, P. Wu, and Y. Zhang, JHEP, **1610**: 136 (2016) [arXiv:1609.00204 [hep-ph]]

16 U. Baur, T. Plehn, and D. L. Rainwater, Phys. Rev. D, **69**: 053004 (2004) [hep-ph/0310056]; A. Papaefstathiou, L. L. Yang and J. Zurita, Phys. Rev. D, **87**(1): 011301 (2013) [arXiv:1209.1489 [hep-ph]]; T. Huang et al, Phys. Rev. D, **96**(3): 035007 (2017) [arXiv:1701.04442 [hep-ph]]; A. Adhikary, S. Banerjee, R. K. Barman, B. Bhattacherjee, and S. Niyogi, arXiv:1712.05346 [hep-ph]

17 M. Maniatis, Int. J. Mod. Phys. A, **25**: 3505 (2010) [arXiv:0906.0777 [hep-ph]]

18 U. Ellwanger, J. F. Gunion, and C. Hugonie, JHEP, **0502**: 066 (2005) [hep-ph/0406215]; U. Ellwanger and C. Hugonie, Comput. Phys. Commun., **175**: 290 (2006) [hep-ph/0508022]

19 P. Bechtle, S. Heinemeyer, O. Stal, T. Stefaniak, and G. Weiglein, Eur. Phys. J. C, **74**(2) 2711 (2014) [arXiv:1305.1933 [hep-ph]]; JHEP, **1411**: 039 (2014) [arXiv:1403.1582 [hep-ph]]; O. Stal and T. Stefaniak, PoS EPS, **-HEP2013**: 314 (2013) [arXiv:1310.4039 [hep-ph]]

20 P. Bechtle, O. Brein, S. Heinemeyer, G. Weiglein, and K. E. Williams, Comput. Phys. Commun., **181**: 138 (2010) [arXiv:0811.4169 [hep-ph]]; Comput. Phys. Commun., **182**: 2605 (2011) [arXiv:1102.1898 [hep-ph]]

21 M. Papucci, K. Sakurai, A. Weiler, and L. Zeune, Eur. Phys. J. C, **74**(11): 3163 (2014) [arXiv:1402.0492 [hep-ph]]

22 S. Kraml, S. Kulkarni, U. Laa, A. Lessa, W. Magerl, D. Proschofsky-Spindler, and W. Waltenberger, Eur. Phys. J. C, **74**: 2868 (2014) [arXiv:1312.4175 [hep-ph]]

23 J. Alwall et al, JHEP, **1407**: 079 (2014) [arXiv:1405.0301 [hep-ph]]; J. Alwall, M. Herquet, F. Maltoni, O. Mattelaer, and T. Stelzer, JHEP, **1106**: 128 (2011) [arXiv:1106.0522 [hep-ph]]

24 T. Sjostrand, S. Mrenna, and P. Z. Skands, JHEP, **0605**: 026 (2006) [hep-ph/0603175]

25 J. de Favereau et al (DELPHES 3 Collaboration), JHEP, **1402**: 057 (2014) [arXiv:1307.6346 [hep-ex]]

26 D. Dercks, N. Desai, J. S. Kim, K. Rolbiecki, J. Tattersall, and T. Weber, Comput. Phys. Commun., **221**: 383 (2017) [arXiv:1611.09856 [hep-ph]]; J. S. Kim, D. Schmeier, J. Tattersall, and K. Rolbiecki, Comput. Phys. Commun., **196**: 535 (2015) [arXiv:1503.01123 [hep-ph]]; M. Drees, H. Dreiner, D. Schmeier, J. Tattersall, and J. S. Kim, Comput. Phys. Commun., **187**: 227 (2015) [arXiv:1312.2591 [hep-ph]]

27 C. Patrignani et al (Particle Data Group), Chin. Phys. C, **40**(10): 100001 (2016)

28 A. Belyaev, M. Drees, O. J. P. Eboli, J. K. Mizukoshi, and S. F. Novaes, Phys. Rev. D, **60**: 075008 (1999) [hep-ph/9905266]

29 M. Aaboud et al (ATLAS Collaboration), JHEP, **1801**: 055 (2018) [arXiv:1709.07242 [hep-ex]]

30 CMS Collaboration, CMS PAS HIG-17-020

31 M. Aaboud et al (ATLAS Collaboration), arXiv:1804.06174 [hep-ex]

32 A. M. Sirunyan et al (CMS Collaboration), Phys. Lett. B, **778**: 101 (2018) [arXiv:1707.02909 [hep-ex]]

33 CMS Collaboration, CMS-PAS-HIG-17-008